STUDY OF HIGHLY PERTURBED SPACECRAFT FORMATION DYNAMICS VIA APPROXIMATION

Ethan R. Burnett[*] and Hanspeter Schaub[†]

This paper explores methods for approximating and analyzing the dynamics of highly perturbed spacecraft formations, with an emphasis on computationally efficient approaches. This facilitates on-board computation or rapid preliminary mission design analysis. Perturbed formation dynamics are often approximated as linear time-varying (LTV) systems, for which Floquet theory can be used to analyze the degree of system instability. Furthermore, the angular momentum of the relative orbital state can be computed with the approximate dynamics to provide additional insight. A general methodology is developed first and then applied to the problem of unstable formation dynamics in asteroid orbits. Here the dominant perturbative effects due to low-order gravitational harmonics and solar radiation pressure are modeled. Numerical simulations validate the approach and illustrate the approximation accuracy achieved.

INTRODUCTION

Spacecraft relative motion dynamics have been a topic of study for nearly 60 years, since the introduction of the well-known Clohessy-Wiltshire[1] linearized model. This model is used for cases of small separation between two spacecraft in Keplerian orbits, with the restriction that the spacecraft about which the relative motion dynamics are linearized is in a circular orbit. There has been much progress in the field since this early work. Many researchers have focused on extending the Clohessy-Wiltshire equations to account for nonzero chief eccentricity or larger formation separation in Keplerian orbits.[2–4] Some work has also been done to analyze the relative motion problem in other coordinate systems, notably curvilinear coordinates and orbit element differences.[5] Additionally, some authors have considered the effects of various perturbations common in planetary orbits, including atmospheric drag,[6] zonal gravity,[7–9] and solar radiation pressure.[10,11] These works are especially valuable for multi-spacecraft formations in low-Earth orbit (LEO) to medium-Earth orbit (MEO). In this region and in other planetary orbits, the scale of the perturbation is small in comparison to the two-body acceleration, but the perturbative effects often still need to be considered.

In the context of relative motion perturbed by gravitational harmonics, notable works include an analysis of perturbed formation flight using quasi-periodic invariant tori,[12] study of J_2-invariant relative motion using mean orbit elements and dynamical constraints,[13] and a newer linearized relative motion model for rotating second degree and order gravity fields.[14] The method of using quasi-periodic invariant tori provides an interesting perspective and compelling results, while differing significantly from the other listed works. The dynamics are not approximated, and the formation

[*]PhD student, Ann and H.J. Smead Department of Aerospace Engineering Sciences, University of Colorado Boulder, CO, 80309

[†]Professor, Glenn Murphy Endowed Chair, Ann and H.J. Smead Department of Aerospace Engineering Sciences, University of Colorado Boulder, CO, 80309

flying problem is approached through dynamical systems theory. Unfortunately, the analysis relies on numerically costly shooting and collocation methods for computing the tori. Methods that are more amenable to fast, on-board implementation are sought. Furthermore, analysis should be extended to consider the simultaneous effects of multiple perturbations as needed, in addition to the low-order zonal harmonics.

Orbits about asteroids and comets are highly affected by the rotating or tumbling gravity field, solar radiation pressure (SRP) disturbances, and other forces such as comet outgassing or thermal radiation pressure from the body. The weaker gravity of these bodies enables these "small" forces to be quite significant to the orbital motion, with an extremely pronounced effect on the scale of relative orbital motion. Two trends in spaceflight suggest that more attention should be paid to studying formation dynamics in such complex environments. First, multi-spacecraft formations are becoming more popular for proposed and actual missions. This is being accelerated by the adoption of CubeSats and low-cost, modular space hardware.[15] Second, asteroids and comets are increasingly chosen as targets for scientific space missions,[16] while private space companies also have interest in these bodies for resource characterization and future extraction.

Operational complexity, light-speed delay, and other issues require future formation-flying asteroid missions to operate autonomously. As a result, it is extremely desirable for computationally efficient, high-accuracy dynamics formulations to be used for on-board navigation and control. This work both surveys existing tools and proposes new approaches for efficient analysis.

This paper explores and applies multiple tools from approximation theory for dealing with the various analytic challenges in highly perturbed spacecraft formation flying. In particular, models obtained using perturbation methods are applied. In addition to their well-known control applications, these analytic models enable a minimal set of dynamically influential parameters to be easily identified, reducing the needed dimensionality of any design-space parameter studies for formation design. Tools from Floquet theory facilitate the stability analysis. By studying how the variation of free parameters in the linearized system matrix affect the system Floquet multipliers, one can obtain dynamical insight about a multi-spacecraft formation, at a fraction of the computational cost of using the original nonlinear system dynamics.

The various techniques introduced in this paper are applied to the approximate linear time-varying (LTV) model of spacecraft relative motion in SRP-perturbed orbits about stably rotating asteroids. The effects of the rotating second degree and order gravity field are also modeled. The results of analytical techniques discussed in this paper are easily interpreted to efficiently predict the parametric variations in formation dynamics and stability.

APPROXIMATING PERTURBED DYNAMICS

Analytic closed-form exact solutions describing perturbed (non-Keplerian) orbital motion do not exist, and numerical simulation of the perturbed dynamics can be computationally expensive. However, approximations do capture some of the complex behavior of the real system, while adopting simple forms that are far more amenable to analysis. The choice of frame of reference or coordinate system affects the ease with which such useful approximations can be obtained, as well as their degree of accuracy.

The focus of this paper is in using linear time-varying (LTV) approximations of the relative motion of two or more spacecraft in similar perturbed orbits. Such approximations describe the differential dynamics of the relative state $\delta X = X_d - X_c$, where the state is a vector of 6 quantities

and the subscripts d and c refer to the spacecraft labeling deputy and chief commonly used in formation flying:

$$\delta \dot{\boldsymbol{X}} = [A(t)]\delta \boldsymbol{X} \tag{1}$$

Note that one may arbitrarily decide which spacecraft is designated as the chief and which is the deputy. Two common representations for the relative state are to resolve the relative position

$$\Delta \boldsymbol{r} = [x, y, z]^\top \tag{2}$$

and velocity

$$\Delta \boldsymbol{r}' = [\dot{x}, \dot{y}, \dot{z}]^\top \tag{3}$$

in a rotating chief-centered local vertical–local horizontal (LVLH) frame, or to use differential orbital elements (chief-centered deviations in an orbit element space). In this context, ( )' denotes the time derivative of a state quantity as seen in the LVLH frame. The results in this paper mainly use the LVLH representation $\delta \boldsymbol{X} = [\Delta \boldsymbol{r}^\top, \Delta \boldsymbol{r}'^\top]^\top$. In this paper, note that δ can represent any difference between any quantities, while Δ is reserved specifically for the relative position and velocity of the deputy as seen from the chief in the rotating frame, and for terms computed solely using these vectors.

This introductory discussion is kept as general as possible to accommodate the diversity of possible environmental perturbations. Resolving the linearized differential dynamics in a perturbed chief-centered frame results in system matrix dependency on the chief state $\boldsymbol{X}_c(t)$, along with perturbative terms $\boldsymbol{\xi}_i(t)$:

$$[A(t)] = \left[A\left(\boldsymbol{X}_c(t), \sum_i \boldsymbol{\xi}_i(t) \right) \right] \tag{4}$$

Note that the perturbative terms typically have dependence on the chief state. This notation reflects the possibility that the system matrix components are factored into perturbed and "unperturbed" quantities. For the LVLH frame description of the differential dynamics, the differential two-body and perturbation accelerations yield kinetic terms. The dependence on the chief state manifests as time-varying kinematic terms which may be described in terms of the perturbed right ascension rate $\dot{\Omega}$ and the argument of latitude rate $\dot{\theta} = \dot{\omega} + \dot{f}$. Except for the secular component of $\dot{\theta}$, the orbit element angular rate terms are on the same order as the perturbations, and are functions of the chief orbit position.

In most situations of interest, the orbital mechanics of the k individual spacecraft in the formation are dominated by simple two-body gravity, but are subject to other significant secondary perturbations. Resolving the perturbative dynamics in terms of associated scaling terms $\alpha_i \ll 1$ that reflect their secondary nature, one may write the state dynamics in terms of two-body gravity ($\boldsymbol{f}_0$) and deviations due to the perturbations:

$$\dot{\boldsymbol{X}}_k = \boldsymbol{f}_0(\boldsymbol{X}_k) + \sum_i \alpha_i \boldsymbol{f}_i(\boldsymbol{X}_k, t) \tag{5}$$

For a finite time span, the solution to these equations is similar to the two-body solution, with $\mathcal{O}(\alpha)$ deviations For example, for a perturbed near-circular orbit, $r(t) \approx a_0(1 + \alpha f(t))$, where $f(t)$ is an approximation of the deviation, and a_0 is the initial orbit semimajor axis. While the chief dynamics are sometimes linear in the small terms α_i, the associated differential dynamics may contain many terms of $\mathcal{O}(\alpha_i^2)$ and higher, due to kinematic term dependence on the perturbed chief orbit position.

These higher-order terms are often neglected for analytic simplicity. For linear model accuracy, it is quite important that no $\mathcal{O}(\alpha)$ terms are missed in the system matrix. Thus, an effort should be made to capture the variations in lone chief orbit terms (e.g. $r(t)$) to $\mathcal{O}(\alpha)$, or to re-initialize the model periodically with updated chief orbit parameters. The approximations of the variations may be obtained through various analytic techniques.[17] It is often the case that the resulting expressions are quasi-periodic, with periods matching the chief orbit period T_c. Thus, one may write:

$$[A(t)] = \left[A\left(\boldsymbol{X}_c(t), \sum_i \boldsymbol{\xi}_i(t) \right) \right] = \left[A\left(\boldsymbol{X}_c(t + T_c), \sum_i \boldsymbol{\xi}_i(t) \right) \right] \tag{6}$$

The perturbative terms $\boldsymbol{\xi}_i$ are $\mathcal{O}(\alpha_i)$ (neglecting higher-order terms) and are also often periodic, with their own associated periods, T_i. If so, then the system matrix $[A(t)]$ will be periodic, with its period being the least common multiple of all periods: $T = \mathrm{LCM}(T_c, T_i)$. Thus, the differential dynamics are written in the useful periodic LTV form:

$$\delta\dot{\boldsymbol{X}} = [A(t)]\delta\boldsymbol{X} = [A(t + T)]\delta\boldsymbol{X} \tag{7}$$

An immediate consequence of this approach is that the degree of instability of uncontrolled spacecraft formations in highly perturbed orbital environments can quickly be characterized – a topic to be explored in the next section. It is comparatively quite easy to analyze or numerically integrate this single linear system instead of working with the original nonlinear perturbed orbital dynamics of an arbitrary number of spacecraft operating in close proximity. Namely, for the linear model, the fundamental relative motion dynamics are deputy-independent, and dependent only on the orbit of a chosen (chief) spacecraft. This approach has many applications for preliminary mission design, maneuver planning, impulsive rendezvous planning, and receding-horizon based closed-loop formation control.

LINEAR ANALYSIS OF FORMATION STABILITY

The previously introduced method of approximation of the perturbed relative motion allows for efficient analysis. This section discusses two approaches. First, linearized analysis using Floquet theory is discussed. Then a new parameter is introduced to describe the evolution of the formation disturbance with time.

Application of Floquet Theory

Floquet theory is a branch of mathematics for analysis of LTV systems $\dot{\boldsymbol{x}} = [A(t)]\boldsymbol{x}$ with periodic system matrices $[A(t)] = [A(t + T)]$. One of the main results of Floquet theory is that it is always possible to transform such a system into one that is LTI via a time-periodic transformation. The resulting LTI system may be easily analyzed using the tools of linear systems theory, and it will share stability properties with the original LTV system.[18] Floquet theory has been used as an analytic tool in work on formation flying before,[19] but the perturbation-based application in this paper is new.

Let $[\Phi(t, t_0)]$ be the state transition matrix (STM) for the LTV system, obtained through analysis or by numerical integration of $[\dot{\Phi}] = [A(t)][\Phi]$ with initial condition $[\Phi(t_0, t_0)] = [I_{6\times6}]$. Since $[A(t)] = [A(t + T)]$, it is clear that $[\Phi(t, t_0)] = [\Phi(t + T, t_0 + T)]$. Using this fact, the state transition matrix from t_0 to $t + T$ can be factored:

$$[\Phi(t + T, t_0)] = [\Phi(t + T, t_0 + T)][\Phi(t_0 + T, t_0)] = [\Phi(t, t_0)][\Phi(t_0 + T, t_0)] \tag{8}$$

The constant matrix $[\Phi(t_0 + T, t_0)]$ is the monodromy matrix.

Floquet theory guarantees the existence of a T-periodic transformation $[P(t)]$, for which it may be assumed $[P(t_0)] = [I_{6\times6}]$:

$$\delta\boldsymbol{X}(t) = [P(t)]\boldsymbol{z}(t) \tag{9}$$

$$\dot{\boldsymbol{z}} = [\Lambda]\boldsymbol{z} \tag{10}$$

$$[P(t)] = [\Phi(t, t_0)]e^{-[\Lambda](t-t_0)} \tag{11}$$

The matrix $[\Lambda]$ has eigenvalues λ_j given in terms of their associated Floquet multiplier ρ_j, which are the eigenvalues of the monodromy matrix:

$$\lambda_j = \frac{1}{T}\ln(\rho_j) = \frac{1}{T}\ln(\mathrm{eig}_j([\Phi(t_0 + T, t_0)])) \tag{12}$$

In this case the matrix $[\Lambda]$ is:

$$[\Lambda] = \frac{1}{T}\ln([\Phi(t_0 + T, t_0)]) \tag{13}$$

Because the periodic transformation $[P(t)]$ is also necessarily bounded, stability of the system in $\delta\boldsymbol{X}$ is the same as that of the system in $\boldsymbol{z}$. The system in $\boldsymbol{z}$ is LTI and easy to analyze. The system stability can also be studied by examining the monodromy matrix directly, through the modulus of the Floquet multipliers. Values of $|\rho_j| < 1$ correspond to stable modes, while $|\rho_j| = 1$ corresponds to T-periodic motion, and $|\rho_j| > 1$ indicates instability.

The system behavior in $\boldsymbol{z}$ is described in terms of the eigenvalues λ_i and eigenvectors $\boldsymbol{\nu}_i$ of $[\Lambda]$:

$$\boldsymbol{z}(t) = \sum_{i=1}^{6} c_i \boldsymbol{\nu}_i e^{\lambda_i(t-t_0)} \tag{14}$$

where in general, the λ_i and $\boldsymbol{\nu}_i$, and c_i may be complex, but $\boldsymbol{z} \in \mathbb{R}^6$.

Due to the transformation initial condition $[P(t_0)] = [I_{6\times6}]$, the initial conditions are identical in both spaces, $\delta\boldsymbol{X}(0) = \boldsymbol{z}(0)$. Thus, the eigenvectors of $[\Lambda]$ correspond to the initial conditions of linearly independent modes in $\boldsymbol{z}$ *and* the transformed motion in $\delta\boldsymbol{X}$, which inherits the stability properties of the modes in $\boldsymbol{z}$.

Within the set of 6 unique eigenvalues, for any complex eigenvalue λ_j, there exists a complex conjugate λ_j^*. Thus, in the case that all 6 eigenvalues are complex, there are only 3 distinct modes. The jth mode is initialized by any real initial condition $\delta\boldsymbol{X}(0) = \boldsymbol{z}(0) = c_j\boldsymbol{\nu}_j + c_j^*\boldsymbol{\nu}_j^*$, where c_j is allowed to be complex.

Constructing $[V]$ column-by-column from the eigenvectors of $[\Lambda]$, and using Eq. (14) at the initial time, one can perform modal decomposition of the relative motion from the initial conditions:

$$\boldsymbol{c} = [V]^{-1}\delta\boldsymbol{X}(0) \tag{15}$$

Here the nonzero coefficients in $\boldsymbol{c} = [c_1, c_2, ..., c_6]^\top$ indicate contribution from the corresponding modes, or complex-conjugate components of modes if the coefficients are complex conjugate pairs.

The transformation of the linearized dynamics into $\boldsymbol{z}$ space enables both stability analysis and modal analysis to be performed on the complex time-varying linearized relative motion dynamics. While the application of these methods is ubiquitous in vibrations research and is also common

some areas of spaceflight such as trajectory generation, the applications in perturbed formation flying dynamics are also extensive and comparatively much less explored. In particular, modal descriptions provide both powerful insights into perturbed formation behavior as well as the potential for engineering applications. As one example, consider that the matrix $[\Lambda]$ may be periodically re-computed as needed, and the periodically updated eigenvectors of its stable modes (if they exist) may be targeted, enabling rendezvous guidance that takes advantage of the perturbed formation dynamics. Such strategy could prove to be much more fuel efficient than impulsive or continuous maneuver strategies that do not account for the perturbed dynamics in this way.

In cases where $[\Phi(t, t_0)]$ can be analytically obtained from the linearized dynamics (typically using symbolic manipulation software), the analytical and applicational opportunities are great.

Systems with Incommensurable Periods and Other Analytic Challenges

The system matrix $[A(t)]$ will often be quasi-periodic, with many chief orbit-periodic terms, along with longer and shorter period terms due to the perturbations. Analysis may be difficult for incommensurable periods of time-varying terms in $[A(t)]$ (e.g. $T_i = 0.6231...T_c$), but this can be remedied to some extent by studying the stability of the closest reasonable commensurable systems (e.g. $T_i = \frac{2}{3}T_c$, thus $T = 2T_c$). For incommensurable periodic perturbations with $T_i \gg$ LCM$(T_c, T_{j \neq i})$ or very short periods $T_i \ll$ LCM$(T_c, T_{j \neq i})$, it may be acceptable to use the initial or averaged perturbation values, respectively. Terms with secular or long-period growth can be replaced by some initial or T-averaged value as needed, but the overall effect of their changing value should be investigated. Reformulations of the problem (for example, a pragmatic choice of coordinates) can also be considered to remove secular terms from the differential dynamics.

The propagation of an uncorrected linearized model of the perturbed formation flying problem will lose accuracy over time, due to both the ignored effects of nonlinearity and the secular growth introduced by approximations that fail to capture multiple time scales in the dynamics. This can be mitigated to some degree, and with varying degree of difficulty, by using other perturbation methods such as the method of multiple scales.[20] However, periodic restarting and re-rectification of chief orbit elements in $[A(t)]$ will also enable such models to be used for long-term close-proximity formation and rendezvous control problems.

Angular Momentum of the Relative Orbital State

Because the relative motion is characterized by time-varying relative position and velocity, a vector quantity that captures large variations in either of these vectors is sought. The angular momentum of the relative orbital state (AMROS) provides an intuitive view of perturbed formation behavior:

$$\Delta \boldsymbol{h} = \Delta \boldsymbol{r} \times \Delta \boldsymbol{r}' \tag{16}$$

It is important to note that this term is not the same as the difference between the angular momentum of the deputy and the chief, $\delta \boldsymbol{h}$. This term is only the component of the angular momentum difference that is purely associated with the chief-centered relative state, and independent of the chief position and velocity:

$$\delta \boldsymbol{h} = \boldsymbol{h}_d - \boldsymbol{h}_c = \Delta \boldsymbol{h} + \left(\boldsymbol{r}_c \times \Delta \boldsymbol{r}' \right) + \left(\Delta \boldsymbol{r} \times \boldsymbol{v}_c \right) \tag{17}$$

A simple argument for using this parameter is that it captures large changes in $\Delta r(t)$ or $\Delta r'(t)$ that indicate significant change to the nature of the relative motion or relative orbit. However,

substitution of the HCW solutions into Eq. (16) provides another argument for the rationale of its use. The result for Δh is expressed in the local radial, transverse, and normal components below:

$$
\begin{aligned}
\Delta h_{\text{HCW}(r)} = {}& -2(3nx_0 + 2\dot{y}_0)z_0 + \frac{2}{n}\dot{x}_0\dot{z}_0 + \left(3\Upsilon z_0\right)\cos nt + n\left(3t\Upsilon - y_0\right)z_0 \sin nt \\
& + \left(-\frac{2}{n}\dot{x}_0 + (y_0 - 3t\Upsilon)\right)\dot{z}_0 \cos nt + \left(2\dot{x}_0 + \frac{3}{n}\Upsilon\dot{z}_0\right)\sin nt
\end{aligned}
\tag{18}
$$

$$
\Delta h_{\text{HCW}(t)} = \dot{x}_0 z_0 + \left(3x_0 + \frac{2}{n}\dot{y}_0\right)\dot{z}_0 + \frac{2}{n}\Upsilon\left(-\dot{z}_0 \cos nt + nz_0 \sin nt\right)
\tag{19}
$$

$$
\begin{aligned}
\Delta h_{\text{HCW}(n)} = {}& -\frac{2}{n}\left(21n^2 x_0^2 + \dot{x}_0^2 + 24nx_0\dot{y}_0 + 7\dot{y}_0^2\right) + \left(2\left(\dot{x}_0^2 + 7\dot{y}_0^2\right) + 3nt\dot{x}_0\Upsilon\right)\frac{\cos nt}{n} \\
& + \left(42n^2 x_0^2 + n\left(49x_0\dot{y}_0 - \dot{x}_0 y_0\right)\right)\frac{\cos nt}{n} - 3\left(\dot{x}_0\dot{y}_0 + n^2 x_0 y_0\right)\frac{\sin nt}{n} \\
& - \left(8nx_0\dot{x}_0 + 2ny_0\dot{y}_0\right)\frac{\sin nt}{n} + \left(9n^2 x_0 t + 6n\dot{y}_0 t\right)\Upsilon\frac{\sin nt}{n}
\end{aligned}
\tag{20}
$$

The term $\Upsilon = 2nx_0 + \dot{y}_0 = 0$ is the linearization of the no-drift condition $\delta a = 0$.[21] For unperturbed close-proximity formations, satisfaction of the no-drift condition manifests in the solution to the linearized dynamics as periodicity of Δh, with the quantity is predicted to be *constant* when the relative motion has no along-track angular offset, parameterized only by nonzero δe and δi:

$$
\Delta \mathbf{h}_{\text{HCW}} = \left(3x_0 + \frac{2}{n}\dot{y}_0\right)\dot{z}_0\hat{\mathbf{e}}_t - \frac{2}{n}\left(21n^2 x_0 + 24nx_0\dot{y}_0 + 7\dot{y}_0^2\right)\hat{\mathbf{e}}_n
\tag{21}
$$

Any violation of the no-drift condition likewise results in Δh no longer being periodic or conserved. Thus, the HCW solution establishes a link between this physical quantity and the linearized approximation of the no-drift constraint. The value of $\Delta h(t)$ using the perturbed linear models will be useful for predicting the degree, timescale, and manner of formation deviation from classical unperturbed geometry. It is important to note that under the true dynamics, Δh is not truly constant for unperturbed chief-centered non-drifting relative motion, but instead fluctuates periodically on a small scale. The scale of these unperturbed fluctuations is a small fraction ($\sim 0.1\%$) of the mean value for formations on any scale that permit linearization. However, the effects of perturbations may result in fluctuations on the same order as the mean.

The expression in Eq. (21) is an angular momentum vector normal to the relative orbit plane, which is fixed in the LVLH frame for unperturbed circular chief orbits. With the presence of small perturbations, the variation of this parameter provides a clear illustration of how the relative orbit grows or shrinks, and how the perturbed relative orbit plane orientation changes. Specifically, this can be done by computing the norm of the deviations $\Delta h(t) - \Delta h(t_0)$, and the time-varying angle between $\Delta h(t)$ and $\Delta h(t_0)$. Due to its transparent relationship to the relative orbital state, it will often be illuminating to perform analysis with the vector quantity Δh.

The stability analysis through Floquet theory describes the modes of the LTV system using the STM for one period T of the system matrix. Assuming that this STM has already been computed for system stability analysis, it can be used to quickly approximate the future relative states at $t = T$ (or any other time $\tau \in [0, T]$ for a given set of initial conditions. Then, the AMROS can be computed for each initial condition, and the difference between $\Delta h(T)$ and $\Delta h(0)$ describes the degree and manner in which the relative motion has been perturbed. The tools of Floquet theory and the AMROS parameter enable rapid parameter studies for identifying conditions for minimal

relative motion instability, while also providing far more analytical insight than surveys with the nonlinear dynamics, all with significantly reduced computational cost.

APPLICATION TO SPACECRAFT FORMATIONS IN ASTEROID ORBITS

In this section, the analytic arguments and techniques developed and reviewed in this paper are applied to the problem of perturbed formation dynamics in orbits around small asteroids. The approximate model is constructed in part using a model accounting for C_{20} and C_{22} recently obtained and tested by one of the authors.[14] The additional linear perturbative terms due to SRP were more recently obtained.[22] To the knowledge of the authors, this is the only linear relative motion model capable of handling the perturbative effects of the C_{22} coefficient. The model is derived such that the perturbed behavior of the chief orbit is approximated by time-varying terms in the system matrix, and the kinematics of relative motion are derived with the effects of the perturbations rigorously accounted for.[23] This methodology yields models with far greater accuracy than models which add perturbative terms to the Clohessy-Wiltshire model in an ad-hoc manner.
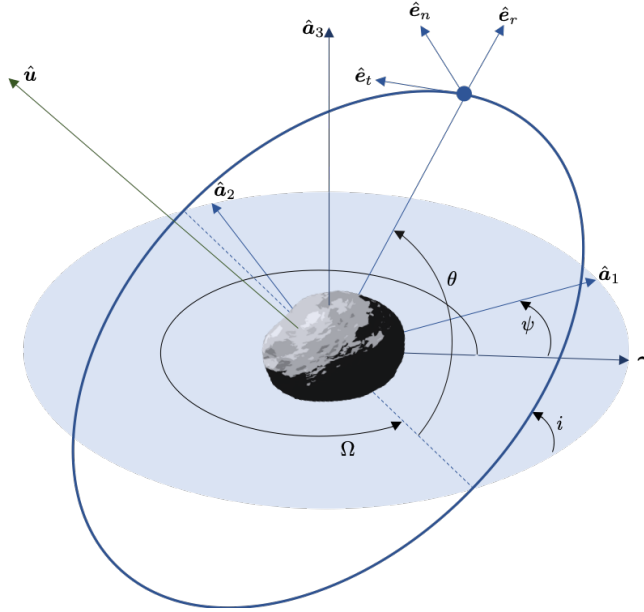

Figure 1: Problem Geometry

Figure 1 shows that the spacecraft orbit is described with respect to the plane perpendicular to the asteroid rotation axis. The axes $\hat{\boldsymbol{a}}_1, \hat{\boldsymbol{a}}_2, \hat{\boldsymbol{a}}_3$ are aligned with the principal axes of inertia of the asteroid, and the asteroid is assumed to be in a spin about the axis of maximum inertia. The right ascension Ω is measured from an inertially fixed reference direction $\boldsymbol{\gamma}$ in this plane, along with the asteroid rotation angle $\psi = \psi_0 + ct$ tracking the $\hat{\boldsymbol{a}}_1$ vector. The vector $\hat{\boldsymbol{u}}$ points towards the sun, and the plane perpendicular to this vector is the terminator plane. It is assumed that the formation is centered about a chief in a near-circular orbit, for which the argument of latitude $\theta = \omega + f$ is a convenient angular coordinate.

The dominant effects of the gravity field (captured by coefficients C_{20} and C_{22}) are accounted for by the linearized model, along with the influence of SRP disturbances, using a body-averaged single-plate SRP model. These terms capture the most important effects for orbits around large

asteroids.[24] Third-body gravity terms are neglected, as the orbit is assumed to be of a radius such that the dominant gravity perturbations are from low degree and order coefficients of the asteroid gravity field, and not from external bodies or particular surface features. The task of including third-body influence in the linearized model will still often be important, so it is left as future work. The effects of the orbit geometry play an important role in the formation dynamics, but the assumptions $r \approx a_0$ and $\theta \approx \theta_0 + nt$ are appropriate for the time span of several orbits, where $n = \sqrt{\mu/a^3}$ is the unperturbed mean motion. The angular rate ratio is defined as $\Gamma = c/n$, R is the Brillouin sphere radius, φ is the asteroid argument of latitude, and h is the orbit angular momentum. The model is given below, in which the kinematics of the perturbed LVLH frame are well-approximated for several orbits, and the perturbed chief orbit parameters may be updated as needed:

$$
\begin{bmatrix} \ddot{x} \\ \ddot{y} \\ \ddot{z} \end{bmatrix} = n^2 \begin{bmatrix} F_{11} & F_{12} & F_{13} \\ F_{21} & F_{22} & F_{23} \\ F_{31} & F_{32} & F_{33} \end{bmatrix} \begin{bmatrix} x \\ y \\ z \end{bmatrix} + \begin{bmatrix} 0 & 2\omega_n & 0 \\ -2\omega_n & 0 & 2\omega_r \\ 0 & -2\omega_r & 0 \end{bmatrix} \begin{bmatrix} \dot{x} \\ \dot{y} \\ \dot{z} \end{bmatrix}
\tag{22}
$$

$$
\begin{aligned}
F_{11} =\ & 3 - \frac{3}{8} C_{20} \left(\frac{R}{a}\right)^2 \left[20 \left(1 - 3\sin^2 i \sin^2 \theta\right) \right] \\
& + \frac{3}{8} C_{22} \left(\frac{R}{a}\right)^2 \left[30 \cos\left(2\left(\Omega - \psi\right)\right) \left(\left(3 + \cos 2i\right) \cos 2\theta + 2\sin^2 i\right) \right. \\
& \left. - 120 \sin\left(2\left(\Omega - \psi\right)\right) \cos i \sin 2\theta \right]
\end{aligned}
\tag{23a}
$$

$$
\begin{aligned}
F_{12} =\ & -6 C_{20} \left(\frac{R}{a}\right)^2 \sin^2 i \sin 2\theta + \frac{3}{4} C_{22} \left(\frac{R}{a}\right)^2 \left[8 \cos\left(2\left(\Omega - \psi\right)\right) \left(3 + \cos 2i\right) \sin 2\theta \right. \\
& \left. + 32 \sin\left(2\left(\Omega - \psi\right)\right) \cos i \cos 2\theta \right]
\end{aligned}
\tag{23b}
$$

$$
\begin{aligned}
F_{13} =\ & -15 \sin i \left(C_{20} \left(\frac{R}{a}\right)^2 \cos i \sin \theta + 2 C_{22} \left(\frac{R}{a}\right)^2 \left[\cos\left(2\left(\Omega - \psi\right)\right) \cos i \sin \theta \right. \right. \\
& \left. \left. + \sin\left(2\left(\Omega - \psi\right)\right) \cos \theta \right] \right) - \frac{a}{nh} N_{\text{SRP}}
\end{aligned}
\tag{23c}
$$

$$
F_{21} = F_{12}
\tag{23d}
$$

$$
\begin{aligned}
F_{22} =\ & 3 C_{20} \left(\frac{R}{a}\right)^2 \sin^2 i \cos 2\theta - \frac{3}{4} C_{22} \left(\frac{R}{a}\right)^2 \left[4 \cos\left(2\left(\Omega - \psi\right)\right) \left(3 + \cos 2i\right) \cos 2\theta \right. \\
& \left. - 16 \sin\left(2\left(\Omega - \psi\right)\right) \cos i \sin 2\theta \right]
\end{aligned}
\tag{23e}
$$

$$
\begin{aligned}
F_{23} =\ & 6 \sin i \left(2 C_{22} \left(\frac{R}{a}\right)^2 \left[\cos\left(2\left(\Omega - \psi\right)\right) \left(\cos i - \Gamma\right) \cos \theta \right. \right. \\
& \left. + \sin\left(2\left(\Gamma - \psi\right)\right) \left(\Gamma \cos i - 1\right) \sin \theta \right] + C_{20} \left(\frac{R}{a}\right)^2 \cos i \cos \theta \left. \right) + \frac{\dot{\varphi}}{n^2} \frac{a}{h} \frac{d}{d\varphi} \left(N_{\text{SRP}}\right)
\end{aligned}
\tag{23f}
$$

$$
F_{31} = F_{13}
\tag{23g}
$$

$$F_{32} = 12C_{22} \left(\frac{R}{a}\right)^2 \Gamma \sin i \left(\cos\left(2\left(\Omega - \psi\right)\right)\cos\theta - \sin\left(2\left(\Omega - \psi\right)\right)\cos i \sin\theta\right)$$

$$- \frac{\dot{\varphi}}{n^2}\frac{a}{h}\frac{d}{d\varphi}\left(N_{\text{SRP}}\right) \tag{23h}$$

$$F_{33} = -1 + \frac{1}{4}C_{20}\left(\frac{R}{a}\right)^2\left[6 + 12\cos^2 i - 30\sin^2 i \sin^2\theta\right]$$

$$+\frac{1}{4}C_{22}\left(\frac{R}{a}\right)^2\left[\cos\left(2\left(\Omega - \psi\right)\right)\left(-15\left(3 + \cos 2i\right)\cos 2\theta - 54\sin^2 i\right)\right. \tag{23i}$$

$$\left.+60\sin\left(2\left(\Omega - \psi\right)\right)\cos i \sin 2\theta\right]$$

The angular velocities of the perturbed LVLH frame are given below:

$$\omega_n = n\left(1 - \frac{3}{4}\left(\frac{R}{a}\right)^2\left[C_{20}\left(1 - 3\sin^2 i \sin^2\theta\right) + 6C_{22}\left(\sin\left(2\left(\Omega - \psi\right)\right)\cos i \sin 2\theta\right.\right.\right.$$

$$\left.\left.\left.-\frac{1}{4}\cos\left(2\left(\Omega - \psi\right)\right)\left(1 + 3\cos 2\theta - 2\cos 2i \sin^2\theta\right)\right)\right]\right) \tag{24}$$

$$\omega_r = 3n\left(\frac{R}{a}\right)^2\sin i\left(2C_{22}\sin\left(2\left(\Omega - \psi\right)\right)\cos\theta + \left[C_{20} + 2C_{22}\cos\left(2\left(\Omega - \psi\right)\right)\right]\cos i \sin\theta\right)$$

$$+\frac{a}{h}N_{\text{SRP}} \tag{25}$$

The term N_{SRP} is the $\hat{e}_n$ component of the SRP disturbance acceleration:

$$N_{\text{SRP}} = -P(R_O)\frac{A}{m}\left(\frac{(1 - \overline{\rho s})}{C_{1(1,1)}} + \overline{a}_2 + 2\overline{\rho s}C_{1(1,1)}\right)C_{1(1,1)}\left(\hat{e}_\xi^\top[C_1(\boldsymbol{\sigma}_r)]^\top\hat{e}_1\right) \tag{26}$$

where $\hat{e}_1 = [1, 0, 0]^\top$ and the unit vector $\hat{e}_\xi$ is not a function of θ due to the problem geometry:

$$\hat{e}_\xi = \begin{pmatrix} \sin\kappa\sin\varphi\cos i - \sin\Omega\cos\varphi\sin i + \cos\Omega\cos\kappa\sin\varphi\sin i \\ \sin\kappa\cos\varphi\cos i + \sin\Omega\sin\varphi\sin i + \cos\Omega\cos\kappa\cos\varphi\sin i \\ \cos\kappa\cos i - \cos\Omega\sin\kappa\sin i \end{pmatrix} \tag{27}$$

with solar radiation pressure terms defined below, for a single-plate model of a spacecraft:

$$P(R_O) \approx \frac{G_1}{R_O^2} \tag{28}$$

$$\overline{a}_2 = \overline{B}(1 - \overline{s})\overline{\rho} + (1 - \overline{\rho})\overline{B} \tag{29}$$

The function $P(R_O)$ is the solar radiation pressure at asteroid orbit distance R_O, and G_1 is the solar radiation force constant at 1 AU. The specular and diffuse reflectivity coefficients are $\overline{s}$ and $\overline{\rho}$, and $\overline{B}$ is the Lambertian scattering coefficient. The model implicitly assumes that the spacecraft orientation with respect to the sun does not change significantly and that the spacecraft orbits are near-circular. It also does not account for eclipse effects without modification.

The matrix $[C_1(\boldsymbol{\sigma}_r)]$ is the rotation matrix from the asteroid-centered Hill frame to the space-craft reference orientation. The primary body Hill frame H_P is defined by orthonormal vectors

$\left\{ \hat{u}, \hat{H} \times \hat{u}, \hat{H} \right\}$, where $\hat{u}$ points toward the sun and $\hat{H}$ is out of the orbit plane of the primary body. In all cases studied here, $[C_1(\boldsymbol{\sigma}_r)] = [I_{3\times3}]$ and thus $C_{1(1,1)} = 1$ (sun-facing). The angle κ is the obliquity of the ecliptic plane and φ is the argument of latitude, or the rotation angle (in the orbit plane) from the Vernal Equinox to the radial vector from the sun to the planet. This model is derived from the facet-based SRP model given by McMahon and Scheeres,[25,26] and is suitable for on-board use. The model assumes that the asteroid is in a circular orbit about the sun, but this could be updated without great difficulty. The timescale of large variations in φ is very slow compared to the orbit period. The motion of the asteroid orbit around the sun is not important here, as these studies focus on short-term formation behavior of $1-5$ orbits, a timescale on the order of days to a week. In this context, terms that are functions of φ are examples of long-period terms that can be ignored by assuming $\varphi \approx \varphi_0$ for the timescale of interest.

Further Analysis of the Linear Model

Note that as $i \to 0$, ignoring long-period SRP effects, the equations of motion can be shown to reduce to the following highly simplified form:

$$\ddot{x} = 3n^2 \left(1 + \frac{5}{2}\alpha + 15\beta \cos\Theta \right) x + 24n^2\beta \sin\Theta y + 2n \left(1 + \frac{3}{4}\alpha - \frac{9}{2}\beta \cos\Theta \right) \dot{y} - \frac{a}{nh} N_{\text{SRP}} z$$

$$\ddot{y} = 24n^2\beta \sin\Theta x - 12n^2\beta \cos\Theta y - 2n \left(1 + \frac{3}{4}\alpha - \frac{9}{2}\beta \cos\Theta \right) \dot{x} + 2\frac{a}{h} N_{\text{SRP}} \dot{z}$$

$$\ddot{z} = -n^2 \left(1 - \frac{9}{2}\alpha + 15\beta \cos\Theta \right) z - 2\frac{a}{h} N_{\text{SRP}} \dot{y}$$

$$(30)$$

where $\alpha = -C_{20} \left(\frac{R}{a} \right)^2$ and $\beta = C_{22} \left(\frac{R}{a} \right)^2$, and $\Theta = 2\big((1-\Gamma)\theta + (\Omega + \Gamma\theta_0 - \psi_0) \big)$. For a purely equatorial orbit $i = 0$, and Ω is undefined, so θ is measured from the reference direction $\boldsymbol{\gamma}$, then $\Theta = 2\big((1-\Gamma)\theta + (\Gamma\theta_0 - \psi_0) \big)$.

Previous analysis in Reference 27 studies these equations without SRP, including their further reduced LTI form for $\Gamma = 1$, and finds that the reduced LTI model can successfully predict the stability properties of the libration points[28] collinear with the $\hat{a}_1$ and $\hat{a}_2$ in the rotating asteroid-fixed frame, and the associated eigenvectors can be used to produce the stable and unstable manifolds. This linearized relative motion model can then be viewed as a generalization of the classical problem of studying motion in the vicinity of equilibrium points in the rotating body-fixed frame.

There is much opportunity for future analysis and extension of this linearized model, both with the current SRP disturbance terms and with future inclusion of third body disturbance terms and other increases in fidelity. The task of deriving and verifying accurate perturbed relative motion models can be challenging. However, the primary purpose of this paper is to demonstrate the analytical and computational utility of such models and the relevance of approximating highly perturbed formation dynamics in this way.

Identifying Important Parameters for Numerical Simulations

The form of Eqs. (23) – (25) lends some insight into important parameters in the formation dynamics. First, note that all C_{22} associated terms are multiplied by either $\cos(2(\Omega - \psi))$ or $\sin(2(\Omega - \psi))$, representing the importance of the evolution of the relative configuration of the orbit plane and the asteroid orientation. For cases of $\Gamma \approx 1$ these terms change slowly, and the

value of $\Omega - \psi_0$ becomes quite important. As the value of Γ is increased (corresponding to a raising of the chief semimajor axis), these terms oscillate more quickly, and the importance of $\Omega - \psi_0$ on formation dynamics is reduced.

Recall that as $i \rightarrow 0$, the in-plane x and y dynamics nearly decouple with the out-of-plane z dynamics, with the exception of one kinetic and two kinematic coupling terms due to the SRP disturbance. The fact that inclination has such an influence on the dynamics suggest that it is also important to consider.

The value of semimajor axis is vitally important to formation dynamics, manifesting through the small parameters premultiplying the time-varying disturbance terms, $C_{2j}(R/a)^2$, $j = 0, 2$. It also affects the magnitude of Γ, determining whether or not the initial relative configuration of the chief orbit and asteroid attitude has an important role.

Lastly, the optical coefficients are important due to their effect on the SRP disturbance, and so is the geometry of the chief orbit with respect to the direction to the sun, captured by the coupled orbit angle terms in $\hat{e}_\xi$ in Eqs. (26) – (27). For simplicity, the studies in this paper assume that the asteroid spin axis orientation is known, along with the spacecraft optical coefficients. The studies consider a family initially near-circular chief orbits (at varying inclinations both near and far from the terminator plane) on which to center the formation. The semimajor axis and inclination are chosen as the main independent parameters for studying the highly perturbed formation dynamics in this problem.

NUMERICAL SIMULATIONS AND ANALYSIS

For the results that follow, close-proximity formation dynamics about a rotating asteroid are considered, with important physical parameters given in Table 1.

Table 1: Important Physical Parameters

Parameters	Values
Asteroid Physical Parameters	$R = 6$ km, $\rho = 2.6$ g/cm^3, $m = 4.9 \times 10^{14}$ kg
Gravity Parameters	$\mu = 3.271 \times 10^{-5}$ km^3/s^2, $C_{20} = -0.0903$, $C_{22} = 0.0375$
Asteroid Orbit Radius	$R_O = 3.5904 \times 10^8$ km (2.4 AU)
Configuration Parameters	$\kappa = 15°$, $\varphi_0 = 90°$, $T_r = 18.0$ hr, $\psi_0 = 0$
Spacecraft Optical Constants	$\frac{A}{m} = 0.3$ m^2/kg, $\overline{B} = 0.6$, $\overline{s} = 0.25$, $\overline{\rho} = 0.3$

The linearized relative motion model in Eq. (22) is used to explore the parameter space for prograde and retrograde near-circular chief orbits. Namely, the inclination of prograde orbits in the terminator plane is $i_T = 75.0°$, and the set of inclinations tested is between $70°$ and $105°$ in one degree increments. The range of Γ tested is from $\Gamma = 3/4$ to $\Gamma = 4$, with 25 evenly spaced values for non-modal analysis results. For the modal analysis, the range is the same but with even increments of $\delta\Gamma = 1/4$. The semimajor axis is related to Γ through the following equation, where $c = 2\pi/T_r$:

$$a = \left(\mu \frac{\Gamma^2}{c^2} \right)^{1/3} \tag{31}$$

For $\Gamma = (3/4, 1, 2, 3, 4)$, the corresponding semimajor axis is $a \approx (12.5, 15.2, 24.1, 31.5, 38.2)$ km. For simplicity, the initial non-critical chief orbit elements $e_0, \omega_0, \Omega_0, f_0$ are all assumed to be zero.

Thus $\theta_0 = 0$ and the chief orbit is initially circular. Small initial nonzero values of chief eccentricity (e.g. $\mathcal{O}(10^{-3})$) do not significantly affect the results. The osculating chief orbit eccentricity is generally of this scale anyway, and can reach higher values in strongly perturbed cases.

While third body effects are ignored in this study, the radius of the asteroid sphere of influence is estimated assuming $m \ll M$:[29]

$$r_{\text{SOI}} = R_O \left(\frac{m}{M} \right)^{2/5} \approx 205 \text{ km} \tag{32}$$

where M is the mass of the sun. Note that at $a = 38.2$ km, the sun's gravity would be a little less than 3% the strength of the asteroid gravity, so the third-body disturbance should be included in the approximate model for higher fidelity in actual applications.

In the studies that follow, for each point in the parameter space, the state transition matrix is computed using the linearized dynamics for one period of the $[A(t)]$ matrix. This enables any type of close-proximity relative motion to be studied without re-integrating each initial condition of interest, and also efficiently provides the monodromy matrix useful for all subsequent computations.

These studies were performed using the Scipy `solve_ivp` function with "BDF" adaptive multi-step variable-order integration settings. The numerical integrator implementations are identical for the linear model and truth model, and simulations with the linear model generally take about one-third of the time of the truth model. This comes with the added benefit of saving the STM history, instead of just the state history from a single initial condition, as is obtained with the truth model.

Studies with AMROS Parameter

First, the magnitude of the maximum deviation (over one orbit) of the AMROS parameter is computed with results from both the linearized model and the truth model. This involves determining the time t at which $\|\Delta \boldsymbol{h}(t) - \Delta \boldsymbol{h}(0)\|$ is maximum, and returning that maximum value. For these results, the relative motion of a single deputy around the chief is considered, with the only nonzero differential elements being $\delta e = 0.003$ and $\delta i = 0.1°$. In the unperturbed case, this would result in periodic bounded planar relative motion with an average separation on the order of 100 meters, with the linear model predicting conservation of $\Delta \boldsymbol{h}$ and the truth model showing small fluctuations.

The results for the highly perturbed asteroid environment are given in Figure 2. The results show strong agreement between the linearized model (left) and truth model (right). The results also establish that within one orbit, the orbits for $\Gamma < 2$ are much more significantly perturbed than higher altitude orbits of $\Gamma > 2$.

Since this figure is used to explore and compare behavior throughout the parameter space, the relative values are more important to study than the absolute values. Both plots show two bands of highly perturbed relative motion behavior around $\Gamma = 1.25$ and $\Gamma = 1.75$, with retrograde orbits ($i > 90°$) showing less deviation than prograde orbits, despite their large angular separation from the terminator plane at $i = 75°$. Overall, the deviations in the AMROS parameter are clearly strongly dependent on the value of the angular rate ratio Γ, with larger deviation for small values of Γ. This shows that the largest deviations from classical relative motion are at low altitude.

Two individual cases from the parameter space serve to illustrate the severity of the perturbations. Recall that the initial relative motion conditions parameterized only by small δe and δi would classically result in bounded relative motion in the absence of these perturbations.[30] First, consider the case from $\Gamma = 1.25$ and $i = 75°$. The relative motion is plotted for 4 orbit periods in Figure 3. The

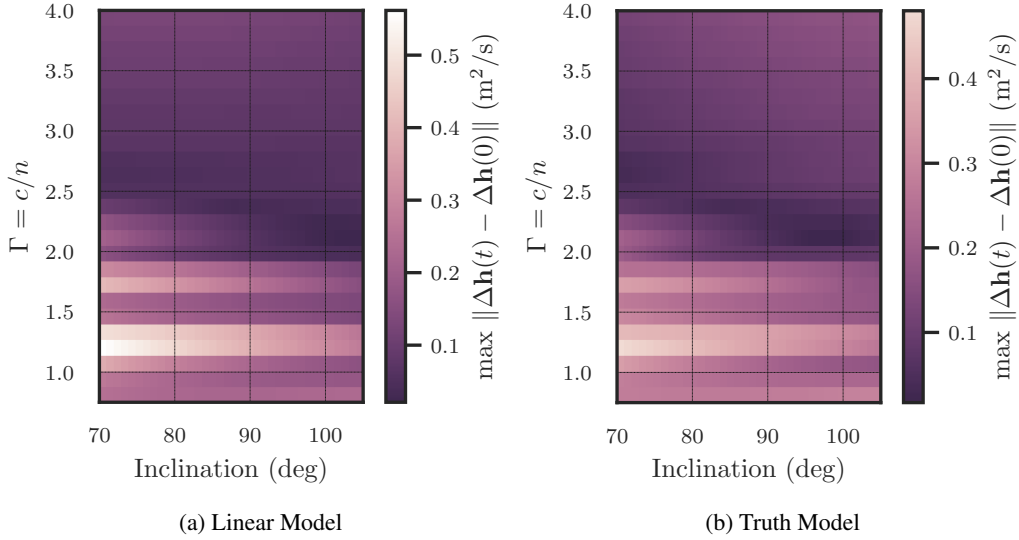(a) Linear Model

(b) Truth Model

Figure 2: Maximum Deviation of AMROS in One Orbit

results show strong agreement for the first orbit, with divergence between the linear and truth model afterwards.

The linear model successfully predicts the degree and manner of the deviation for the first orbit. The truth model shows that over the course of the next several orbits, the deputy continues to rapidly drift further away. This long-term behavior is not well captured by the linear model – at least not without periodically updating the chief orbit elements and re-initializing. Such an update and re-initialization procedure would be reasonable in any on-board guidance implementation procedure, but these results evaluate the efficacy of the unaided model. The eventual failure of the model is an unsurprising phenomenon, given the rapid change in geometry and scale of the true motion. What is most surprising is the rapid timescale and manner in which a close-proximity two space-craft formation is ripped apart by the dynamics of the orbital environment. This is not an isolated case: sampling other bright regions in Figure 2 often results in finding similar highly destabilized behavior.

To investigate a region in the parameter space where the maximum deviation of the AMROS parameter is comparatively rather low, the case of $\Gamma = 2$ and $i = 95°$ is chosen. The relative orbital motion is plotted in Figure 4. The resulting relative motion is indeed more stable for short time spans, and the behavior is well-approximated (without any re-initialization and chief orbit parameter updates) for 4 orbits. Since the orbit period in this case is 36 hours, this stable behavior persists and is well-approximated for 6 days. The long-term relative motion is however still highly unstable, as can be seen from the truth model results propagated over 10 orbits.

The individual case results in Figures 3 and 4 reflect general observations that the maximum deviation of the AMROS parameter is a good tool for studying short-term behavior. As discussed, this parameter can also be used to study how the relative orbit plane changes over time, but such results are omitted to make room for other results.

These results show that the behavior of the AMROS parameter predicted by the linearized dynamics can be used to describe perturbation and destabilization of close-proximity relative motion
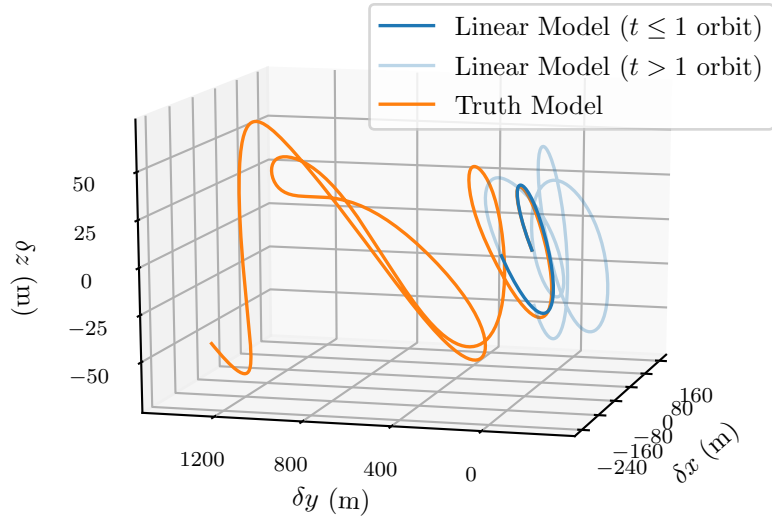
Figure 3: Perturbed Relative Motion with $\Gamma = 1.25$, $i = 75°$

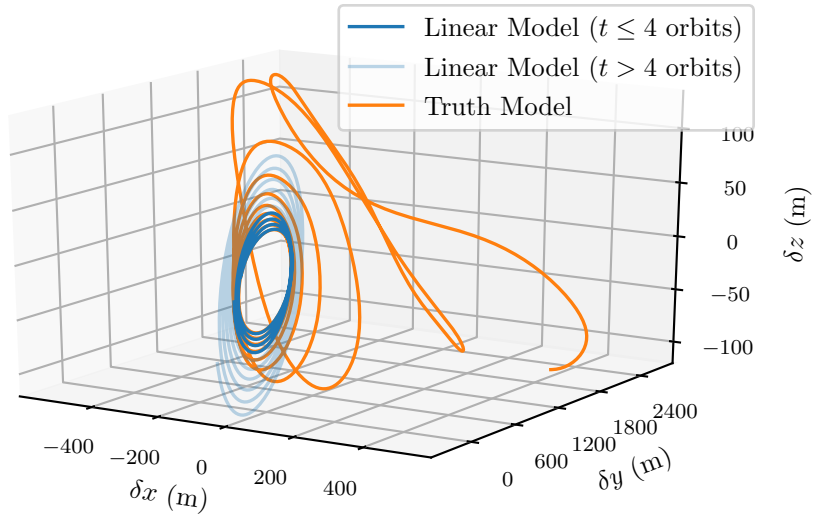**Figure 4**: Perturbed Relative Motion with $\Gamma = 2.0$, $i = 95°$

in the short term, but the long-term behavior is also of interest. The case used to produce Figure 4 shows that short-term stable behavior can still become destabilized in the long-term. In light of these results, it is natural to ask if the approximate dynamics can be used to easily identify cases where relative motion will be stable for much longer time spans. It turns out that this is also possible.

Using Tools from Floquet Theory and Modal Analysis

The linearized model is capable of providing much more information if the preceding results are combined with other approaches discussed in this paper. The analysis in this section uses the monodromy matrix and studies the stability of the LTI transformed system in z, along with the fundamental relative orbital motion modes predicted by the linearized model. These provide a wealth of information about the system behavior throughout the parameter space.

15

Figure 5 shows the variation of the modulus of the largest Floquet multiplier in the parameter space. Recall that the Floquet multipliers are eigenvalues of the monodromy matrix. Any Floquet multiplier with a modulus greater than 1 is an indicator of the potential for system instability. Stability can only be ensured only if $|\rho_j| \leq 1 \; \forall j$. The data in Figure 5 does not provide a complete parameterization of the degree of instability by itself. The figure does not show how many unstable modes exist; it only shows the severity of the most unstable mode. However, the figure still provides useful insights into the potential for instability depending on the value of Γ and i. It is worth noting that the two horizontal bands in the figure are somewhat reminiscent of the data in Figure 2. For cases with a highly unstable mode, a given initial condition (such as the initial conditions used to generate Figure 2) will likely partially excite the unstable mode as well – resulting in rapid relative motion destabilization. This could explain the correlation of the two horizontal bands.
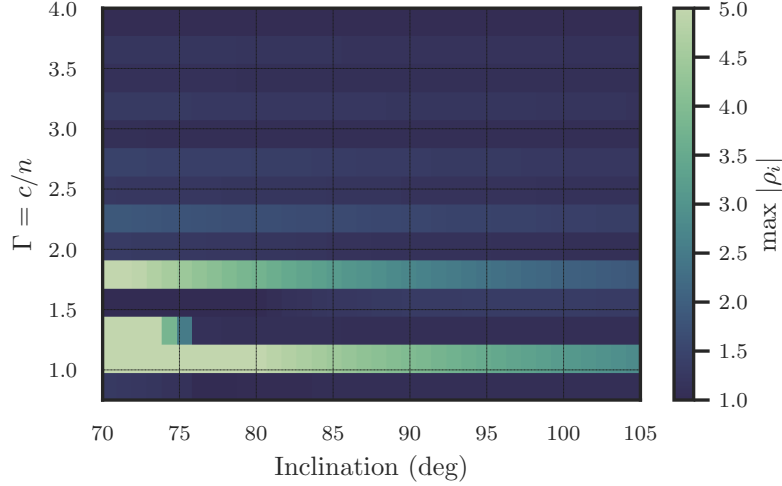

Figure 5: Modulus of Largest Floquet Multiplier

For weakly unstable systems with all $|\rho| \approx 1$, the destabilization that occurs by partial projections of the initial condition into the unstable subspace is less rapid than for systems with a multiplier $|\rho| \gg 1$. Furthermore, formation geometry selected to avoid exciting the unstable modes will enable the motion to remain within specified bounds for longer without corrective maneuvers. Thus, uncorrected formation stability will still be dependent on the initial conditions of relative states of the spacecraft. This would be very expensive to study with simulations using the truth model alone. However, parameter studies with the linear system can efficiently provide this insight, since the linear dynamics of the perturbed relative motion can be decomposed into linearly independent modes in z space. Recall that since $\delta X = [P(t)]z$ and $[P(t_0)] = [I_{6\times6}]$, the behavior of the fundamental modes can be represented in δX coordinates as well.

The approximate model is first used to determine how the number of relative motion modes varies in the parameter space. This data is presented in Figure 6(a).

It is also useful to consider how many of these modes are highly unstable. The approach in this work is to determine if the real part of any of the eigenvalues of $[\Lambda]$ exceeds a critical value λ^*, defined below as the minimum value required for the real exponential term in the $z(t)$ solution to increase by a factor of e in N orbits:
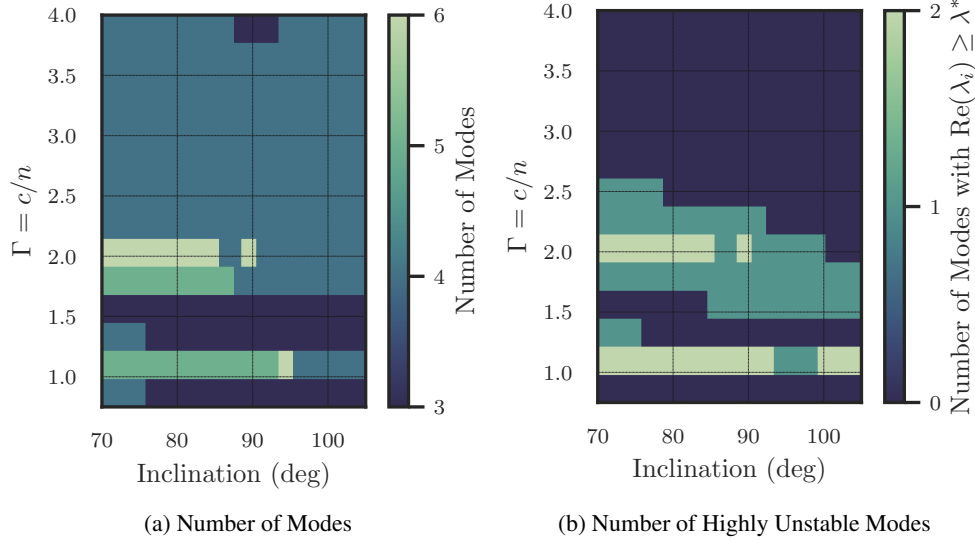
$$\lambda^* = \frac{c}{2\pi\Gamma N} \tag{33}$$

(a) Number of Modes

(b) Number of Highly Unstable Modes

Figure 6: Relative Orbital Motion Modal Data

(a) $i = 75°$. Stable Modes: 1, 2, 3; Unstable: 4, 5, 6   (b) $i = 95°$. Stable Modes: 1, 2; Unstable: 3, 4
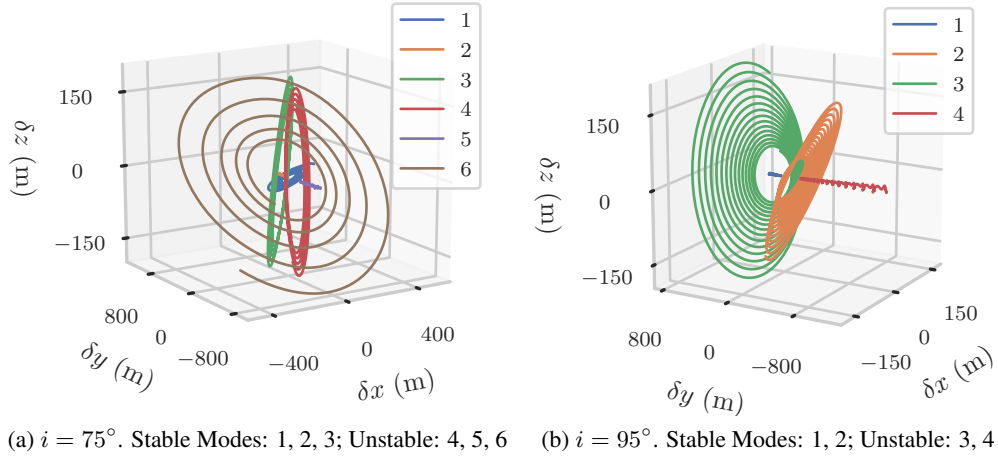
Figure 7: Relative Motion Modes for $\Gamma = 2$

Setting $N = 10$, this is of $\mathcal{O}(10^{-6})$ for much of the parameter space surveyed.

The critical value λ^* is used to create Figure 6(b). It is important to keep the limitations of the model in mind when interpreting these modal results. The relative duration of model accuracy is highly correlated with the relative magnitude of maximum deviation in the AMROS parameter. In the most highly perturbed regions of the parameter space (lower values of Γ), the linear model only predicts initial behavior well without re-initialization and update of perturbed chief orbit parameters. The stability predictions below $\Gamma = 1.5$ are not consistently trustworthy. Figure 6(b) predicts that generally for high-altitude orbits, there are no highly unstable modes, and this property extends to progressively lower orbits as inclination is increased to polar and retrograde orbits.

Since all solutions of the linear model will be a superposition of the fundamental modes, vari-

ations in the modal behavior at intermediate levels of Γ are complex and worth investigating. At $\Gamma = 2$, the number of total modes and their stability properties vary with inclination. This is illustrated by Figure 7. Note that scale is irrelevant for these linear results. For relative motion centered in the orbit with $i = 75°$, there are 6 unique modes, and all eigenvalues are real. These are plotted for 5 orbits. Three modes are unstable, and two are highly unstable (modes 5 and 6). Mode 4 is slightly unstable ($\lambda_4 = 5.07 \times 10^{-7}$) and mode 3 is stable ($\lambda_3 = -5.06 \times 10^{-7}$). Modes 1 and 2 are strongly stable. Modes 2 and 5 are distorted along-track motion. Such modes appear throughout much of the parameter space, but their eigenvectors are poorly scaled, and do not accurately represent the motion of the system for long time spans. However, modes such as 1, 3, 4, and 5 do reflect the actual formation dynamics. These modes (or mixtures of them) could be periodically re-computed and targeted by a guidance system to enforce desired relative motion behavior.

Figure 7(b) shows the modes for relative motion about a chief with $i = 95°$, plotted for 15 chief orbits. These represent the fundamental modes of the same point in the parameter space used to generate Figure 4. The eigenvalues corresponding to each mode are all of scale 10^{-7}, with multiplying factors $\lambda_1 = -9.1, \lambda_2 = -6.6 \pm 2.5i, \lambda_3 = 6.6 \pm 2.6i, \lambda_4 = 9.2$. From these results, it is evident that the initial condition of the motion in Figure 4 has partially excited the unstable third mode.
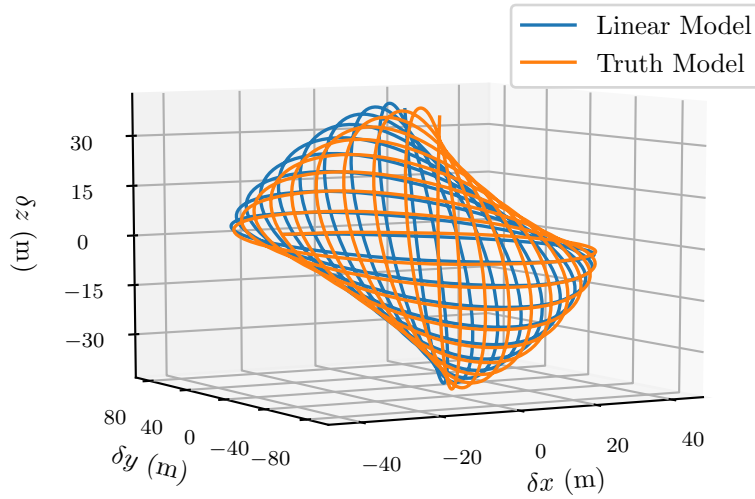

Figure 8: Long-Term Stable Relative Motion Mode

Long-term accurate prediction is possible without any model re-initialization for cases where the relative motion is not too perturbed to compromise model accuracy. This is incredibly useful, as it can be used to find relative motion conditions that would result in bounded formations with linearly predictable behavior for very long time spans without correction. Figure 6 shows that for values of $\Gamma > 2.5$, there are only 3 or 4 relative motion modes, and none are particularly unstable. Selecting $\Gamma = 4.0$ and $i = 75°$, the modal results indicate that there are two along-track modes (one stable and one unstable) and two very similar modes with eigenvalues $\lambda_{2,3} = \pm 9.7 \times 10^{-9} \pm 6.1 \times 10^{-7}i$. This represents stable relative motion for long time spans, due to the very small real parts of the eigenvalues. Figure 8 is produced by initializing the mode with the eigenvalue with the slightly negative real part. The initial condition is just the associated eigenvector with a chosen scaling,

given below in LVLH components in meters and meters/second:

$$\delta \boldsymbol{X}_0 = c\boldsymbol{\nu} = \left(12.5,\ 7.90,\ 0.8,\ 9.69 \times 10^{-4},\ 6.05 \times 10^{-4},\ 7.27 \times 10^{-5}\right)^{\top} \qquad (34)$$

The first half-period of behavior is shown, amounting to approximately 10 chief orbit periods. There is a positive rotation of the relative orbit about the $\hat{\boldsymbol{e}}_r$ vector and a shrinking of the relative position bounds along $\hat{\boldsymbol{e}}_r$. The approximate model agrees with the true behavior for 10 orbits (30 days), with some growing distortion visible. The dynamics in this region of the parameter space are clearly favorable for fuel-efficient close-proximity formation flying. Overall, the results of modal analysis provide a wealth of insight into the behavior of uncontrolled close-proximity relative motion.

CONCLUSIONS

This paper introduces methods and tools for using approximate models of relative motion dynamics to study the behavior of close-proximity spacecraft motion in highly-perturbed environments. Many of these tools are already commonly used in other fields, but are comparatively unused in formation flying. The methods are discussed generally and then applied to the problem of multi-spacecraft formations in asteroid orbits. Formation design and rendezvous planning is more difficult in such environments than in planetary orbits, since the perturbations dramatically affect the uncontrolled relative motion dynamics in complex ways. This is demonstrated by parameter studies showing the deviation of the angular momentum of the relative orbital state (AMROS), and by simulation of individual cases from this parameter study.

Results with an approximate model show that the analytical approaches discussed provide a wealth of information not easily obtained through studies using a truth model. When propagated without correction, the model still provides enough dynamical information to identify orbit conditions that permit long-term stable formations. Use of tools from Floquet theory also permits modal analysis of the perturbed relative motion, providing a significant boost in understanding of safe and unsafe formation design in highly perturbed environments.

Opportunities for future work include both expanding the current studies to consider other environments, and improving the given relative motion model fidelity and efficacy. In particular, the effects of additional perturbations could be explored, such as third-body gravity. Efficient methods for periodic model updating and correction could also be applied. In addition, a formation and rendezvous guidance implementation of such models could be developed and demonstrated. This could be applied in a future mission using either low-thrust or by exploiting attitude-dependent variations in the solar radiation pressure (SRP) force, since the forces required to change and maintain small formations are typically very small in orbits around asteroids and other small bodies.

ACKNOWLEDGEMENTS

REFERENCES

[1] W. H. Clohessy and R. S. Wiltshire, "Terminal Guidance System for Satellite Rendezvous," *Journal of the Aerospace Sciences*, Vol. 27, Sept. 1960, pp. 653–658.
[2] J. P. DeVries, "Elliptic Elements in Terms of Small Increments of Position and Velocity Components," *AIAA Journal*, Vol. 1, Nov. 1963, pp. 2626–2629.
[3] R. G. Melton, "Time-Explicit Representation of Relative Motion Between Elliptical Orbits," *AIAA Journal of Guidance, Control, and Dynamics*, Vol. 23, No. 4, 2000, pp. 604–610.

[4] C. D. Karlgaard and F. H. Lutze, "Second Order Relative Motion Equations," *Journal of Guidance, Control, and Dynamics*, Vol. 26, No. 1, 2003, pp. 41–49.

[5] H. Schaub, "Relative Orbit Geometry Through Classical Orbit Element Differences," *AIAA Journal of Guidance, Control, and Dynamics*, Vol. 27, Sept.–Oct. 2004, pp. 839–848.

[6] T. Carter and M. Humi, "Clohessy-Wiltshire Equations Modified to Include Quadratic Drag," *Journal of Guidance, Control, and Dynamics*, Vol. 25, November-December 2002, pp. 1058–1063.

[7] S. A. Schweighart and R. J. Sedwick, "High-Fidelity Linearized J Model for Satellite Formation Flight," *AIAA Journal of Guidance, Control, and Dynamics*, Vol. 6, Nov. 2002, pp. 1073–1080.

[8] E. R. Burnett, E. A. Butcher, A. J. Sinclair, and T. A. Lovell, "Linearized Relative Orbital Motion Model About an Oblate Body Without Averaging," *AAS/AIAA Astrodynamics Specialist Conference*, American Astronautical Society, 2018.

[9] A. D. Biria and R. P. Russell, "A Satellite Relative Motion Model Including J_2 and J_3 via Vinti's Intermediary," *Celestial Mechanics and Dynamical Astronomy*, Vol. 130, No. 23, 2018.

[10] T. Guffanti, S. D'Amico, and M. Lavagna, "Long-Term Analytical Propagation of Satellite Relative Motion in Perturbed Orbits," *AAS/AIAA Astrodynamics Specialist Conference*, 2017.

[11] K. Parsay and H. Schaub, "Drift-Free Solar Sail Formations in Elliptical Sun-Synchronous Orbits," *Acta Astronautica*, Vol. 139, 2016, pp. 201 – 212.

[12] N. Baresi, *Spacecraft Formation Flight on Quasi-periodic Invariant Tori*. PhD thesis, University of Colorado Boulder, 2017.

[13] H. Schaub and K. T. Alfriend, "J_2 Invariant Relative Orbits for Spacecraft Formations," *Celestial Mechanics and Dynamical Astronomy*, Vol. 79, No. 2, 2001, pp. 77–95.

[14] E. R. Burnett and E. A. Butcher, "Linearized Relative Orbital Motion Dynamics in a Rotating Second Degree and Order Gravity Field," *AAS/AIAA Astrodynamics Specialist Conference*, American Astronautical Society, 2018.

[15] C. Araguz, E. Bou-Balust, and E. Alarcon, "Applying autonomy to distributed satellite systems: Trends, challenges, and future prospects," *Systems Engineering*, Vol. 21, 2018, pp. 401–416.

[16] P. Michel, M. Kueppers, A. Cheng, and I. Carnelli, "The HERA Mission: European Component of the Asteroid Impact and Deflection Assessment (AIDA) Mission to a Binary Asteroid," *49th Lunar and Planetary Science Conference*, 2018.

[17] D. Brouwer, "Solution of the Problem of Artificial Satellite Theory Without Drag," *The Astronomical Journal*, Vol. 64, No. 1274, 1959, pp. 378–397.

[18] A. H. Nayfeh and D. T. Mook, *Nonlinear Oscillations*. John Wiley & Sons, Inc., 1979.

[19] G. Inalhan, M. Tillerson, and J. P. How, "Relative Dynamics & Control of Spacecraft Formations in Eccentric Orbits," *AIAA Journal of Guidance, Control, and Dynamics*, Vol. 25, Jan.–Feb. 2002, pp. 48–59.

[20] C. M. Bender and S. A. Orszag, *Advanced Mathematical Methods for Scientists and Engineers: Asymptotic Methods and Perturbation Theory*. Springer-Verlag, 1991.

[21] H. Schaub and J. L. Junkins, *Analytical Mechanics of Space Systems*. Reston, VA: AIAA Education Series, 4th ed., 2018.

[22] E. R. Burnett and H. Schaub, "Spacecraft Formation and Orbit Control Using Attitude-Dependent Solar Radiation Pressure," *International Workshop on Satellite Constellations and Formation Flying*, IAF Astrodynamics Committee, 2019.

[23] S. Casotto, "The Equations of Relative Motion in the Orbital Reference Frame," *Celestial Mechanics and Dynamical Astronomy*, Vol. 124, No. 3, 2016, pp. 215–234.

[24] D. J. Scheeres, *Orbital Motion in Strongly Perturbed Environments*. Springer-Verlag Berlin Heidelberg, 2012.

[25] D. J. Scheeres, "The dynamical evolution of uniformly rotating asteroids subject to YORP," *Icarus*, Vol. 188, 2007, pp. 430–450.

[26] J. W. McMahon and D. J. Scheeres, "New Solar Radiation Pressure Force Model for Navigation," *Journal of Guidance, Control, and Dynamics*, Vol. 33, No. 5, 2010, pp. 1418–1428.

[27] E. Burnett, "Relative Orbital Motion Dynamical Models for Orbits about Nonspherical Bodies," Master's thesis, University of Arizona, 2018.

[28] W. M. Kaula, *Theory of Satellite Geodesy : Applications of Satellites to Geodesy*. New York: Dover Publications, Nov. 2000.

[29] R. H. Battin, *An Introduction to the Mathematics and Methods of Astrodynamics*. New York: AIAA Education Series, 1987.

[30] K. T. A. e. al., *Spacecraft Formation Flying*. Elsevier, 2010.